Article

Vibrational biospectroscopy characterises biochemical differences between cell types used for toxicological investigations and identifies alterations induced by environmental contaminants

Heys, Kelly A., Shore, Richard F., Pereira, M. Glória and Martin, Francis L

Environmental Toxicology and Chemistry

Environmental Toxicology

VIBRATIONAL BIOSPECTROSCOPY CHARACTERISES BIOCHEMICAL DIFFERENCES BETWEEN CELL TYPES USED FOR TOXICOLOGICAL INVESTIGATIONS AND IDENTIFIES ALTERATIONS INDUCED BY ENVIRONMENTAL CONTAMINANTS

KELLY A. HEYS, RICHARD F. SHORE, M. GLÓRIA PEREIRA, and FRANCIS L. MARTIN

Environ Toxicol Chem., **Accepted Article** • DOI: 10.1002/etc.3890

Accepted Article

Environmental Toxicology **Environmental Toxicology and Chemistry**
DOI 10.1002/etc.3890

VIBRATIONAL BIOSPECTROSCOPY CHARACTERISES BIOCHEMICAL DIFFERENCES BETWEEN CELL TYPES USED FOR TOXICOLOGICAL INVESTIGATIONS AND IDENTIFIES ALTERATIONS INDUCED BY ENVIRONMENTAL CONTAMINANTS

KELLY A. HEYS,[a,b] RICHARD F. SHORE,[b] M. GLÓRIA PEREIRA,[b] and FRANCIS L. MARTIN[a,c*]

[a] Lancaster Environment Centre, Lancaster University, Bailrigg, Lancaster, UK

[b] Centre of Ecology and Hydrology, Lancaster University, Bailrigg, Lancaster, UK

[c] School of Pharmacy and Biomedical Sciences, University of Central Lancashire, Preston, UK

***Address correspondence to:**

E-Mail: flmartin@uclan.ac.uk

This article contains online-only Supplemental Data

Submitted 18 March 2017; Returned for Revision 25 April 2017; Accepted 16 June 2017

Abstract: The use of cell-based assays is essential in reducing the number of vertebrates used in the investigation of chemical toxicities and in regulatory toxicology assessment. An important factor in obtaining meaningful results which can be accurately extrapolated is the use of biologically appropriate cell lines. In this preliminary study, ATR-FTIR spectroscopy with multivariate analysis was used to assess the fundamental biomolecular differences between a commonly used cell line, MCF-7 cells, and an environmentally relevant cell line derived from Mallard (*Anas platyrhynchos*) dermal fibroblasts. To better understand differences in basic cell biochemistry, the cells were analysed in the untreated state or post-exposure to PCB and PBDE congeners. The main spectral peaks in spectra from both cell types were associated with cellular macromolecules, particularly proteins and lipids but the spectra also revealed some cell-specific differences. Spectra from untreated Mallard fibroblasts spectra contained a large peak associated with lipids. The cell-related differences in lipid and DNA were also identified as regions of spectral alteration induced by PBDE and PCB exposure. Although lipid alterations were observed in post-treatment spectra from both cell types, these may be of more significance to Mallard fibroblasts, which may be due to increased intracellular lipid as determined by Nile red staining. Untreated MCF-7 cell spectra contained unique peaks related to DNA and nucleic acids. DNA associated spectral regions were also identified as areas of considerable alteration in MCF-7 cells exposed to some congeners including PBDE 47 and PCB 153. The findings indicate that in their native state, MCF-7 and Mallard cells have unique biochemical differences, which can be identified using ATR-FTIR spectroscopy. Such differences in biochemical composition differences, which may influence cell susceptibility to environmental contaminants and therefore influence the choice of cell type used in toxicology experiments. This is the first study to analyse the biochemistry of a Mallard dermal fibroblast cell line and to use ATR-FTIR spectroscopy for this purpose. ATR-FTIR spectroscopy is demonstrated as a useful tool for exploration of biomolecular variation at the cellular level and with further development, it could be used as part of a panel of cell-based assays to indicate when different results might be seen in environmental species compared to currently used cell lines. This article is protected by copyright. All rights reserved

Keywords: Biospectroscopy; Cell-specific differences; Mallard fibroblasts; MCF-7 cells; Regulatory toxicology; Spectral alterations

INTRODUCTION

In order to protect the health of humans and wildlife, it is important that we are able to understand and estimate the toxicity of contaminants that enter the environment. To date, this has been made possible using biological and computational models that allow us to study the effects of such contaminants at various levels within an organism [1]. For regulatory purposes, it is crucial that the toxicity of pollutants is fully characterised as regulatory guidelines determine the usage of chemicals which may enter the environment [2][3]. Therefore, it is essential that we have accurate methodologies in place that allow us to assess the effects of contaminant chemicals in experimental and regulatory contexts. Current methods used to assess the effects of exposure to chemicals can be time-consuming, expensive or rely on a high degree of operator competence. Therefore, considerable effort is being invested into developing new tools for these purposes.

Attenuated total reflection-Fourier transform infrared (ATR-FTIR) spectroscopy is a high throughput and economical technique that has been used for analyses in several fields including biomedicine [4], geology [5], plant science [6] and ecotoxicology [7]. ATR-FTIR is a vibrational spectroscopy technique that can characterise biomolecules in samples by measuring the absorption of infrared (IR) by IR-active chemical bonds through their inherent dipole moment [8]. The dipole moments occur at specific wavelengths depending on the chemical bonds present. This data not only confers structural or conformational information but also by looking at alterations of specific bonds between biological samples, further information such as toxic effects of chemicals can be elucidated [9]. It has previously been recognised that ATR-FTIR and other vibrational spectroscopy techniques may be useful to study the effects of chemical toxicants in biological systems [10]. It has been used to investigate the effects of environmental contaminants including fungicides [11], nanoparticles [12] and polycyclic aromatic hydrocarbons

(PAHs) [13] as well as being used to investigate composition of contaminants in mixtures [14], mixture interactions [15] and the biological toxicity of environmental binary mixtures [16]. ATR-FTIR spectroscopy is highly useful as it can be used to investigate the toxicity of chemicals using a wide range of biological substrates, both live and fixed, including biofluids, tissues and cells [17].

In vitro cell models are an increasingly emerging focus for toxicity research, including that using vibrational spectroscopy. Toxicity testing is required to understand how chemicals in the environment can affect organisms but the methods by which we experimentally determine an agent's toxicity and at which concentrations is a topic of some debate. The use of animal models is regarded by many as most representative as it provides toxicity information within the complexity of the whole-organism level [18]. However, as set out by The National Centre for the Replacement, Refinement and Reduction of Animals in Research (NC3R), we must reduce the number of vertebrates used in scientific procedures and *in vitro* toxicity testing has historically been a precursor for animal testing. In the wake of the NC3R guidelines, chemical testing using cell lines has been increasingly used as a suitable surrogate [19]. Analysis of toxicity at this level has the benefit of capturing important interactions between the chemical and biological targets which happens first in the cells, before an organ or tissue effect is seen [20]. On the other hand, many of the cell lines used for environmental toxicant studies are often far removed from the cell types that would be exposed to chemicals in sentinel organisms. Using commonly employed cell lines does have the benefit that the cells are well characterised but problems may arise during the interpretation of results in how these are extrapolated to meaningful conclusions regarding whole organism toxicity. Additionally, in the context of environmental research, there are many species groups, *e.g.*, mammals, birds, fish and amphibians, which comprise many physiological and

biochemical differences that can further complicate extrapolation of experimental results [21]. It is possible that current experimental cell lines, which may come from very different test organisms or be derived from abnormal tissues such as tumours, are not the most representative system in which to measure how a chemical contaminant will affect environmental species. The development of new cell lines, from environmentally relevant sources, could represent a new focus for investigating the toxicity of environmental contaminants [22].

The major aim of this study was to compare and evaluate two cell lines which may be used for testing the toxicity of environmental contaminants; an MCF-7 cell line which has been used for such experiments [23, 24] and a Mallard (*Anas platyrhynchos*) dermal fibroblast cell line derived from free-living birds, representing a test system which is biologically closer to wildlife species found in the environment. Mallard dermal fibroblasts were selected as a preliminary test cell line as they are non-mammalian, from an environmentally abundant species and in an anatomical site, which would frequently come into contact with contaminants. Environmentally relevant cell lines, such as this, may provide results that can be more accurately extrapolated to environmental organisms, either when used alone or in conjunction with other cell lines. Both the fundamental biochemistry of the cells and their response to chemical contaminant exposure was analysed using ATR-FTIR spectroscopy with computational analysis methods. As described, ATR-FTIR spectroscopy is a sensitive technique which is able to differentiate between cell and tissue types [9] and therefore was used to determine cellular differences at the biomolecular level. In order to determine whether there were differences in response post-exposure to common environmental contaminants which may necessitate the use of alternative cell lines, the cells were treated with PCB 153 and PBDE congeners 47, 99 and 153 which are well-known environmental pollutants. Treatments with single agents at environmentally reported

concentrations were used to simulate environmental levels. The results of studies like this may be essential for the development of accurate cell-based assays, particularly for understanding how environmental chemicals are toxic to avian species.

METHODS AND MATERIALS

Test agents

Stock solutions of PBDE congeners 47, 99 and 153 were purchased, pre-dissolved in nonane at a concentration of 50 µg/mL, from LGC standards (Teddington, UK). PCB 153 was purchased as a powder from Greyhound Chromatography and Allied Chemicals (Birkenhead, UK) and made up in nonane (Sigma-Aldrich, Dorset, UK). Stock solutions for chemical treatments were made up to a concentration of 2 µM in DMSO and then serially diluted in DMSO to achieve the experimental concentrations required. Vehicle controls consisted of the same amount of DMSO as used in chemical treatments, spiked with equal quantities of nonane.

Cell culture

Human MCF-7 cells were taken from an established culture derived from a frozen aliquot from a line gifted by the Institute of Cancer Research. For experiments, they were grown in Dulbecco's modified essential medium (DMEM) supplemented with 10% heat-inactivated fetal bovine serum (FBS) and a penicillin and streptomycin mixture (100 U/mL and 100 µg/mL respectively). Mallard (*Anas platyrhynchos*) dermal fibroblasts (derived as previously described [25]) were grown in the same medium with the addition of 2% chicken serum (Sigma-Aldrich) and 1% non-essential amino acids (Thermo Fisher Scientific, Nottinghamshire, UK). Both cell types were cultured in a humidified atmosphere with 5% CO_2 in air, at a temperature 37°C. Cells were sub-cultured twice weekly by disaggregation with trypsin (0.05%)/EDTA (0.02%) solution before spinning at 1000 × g for 5 minutes. The resultant cell pellet was then re-suspended in

fresh complete DMEM and seeded into T75 flasks for routine sub-culture or T25 for experiments. Unless stated otherwise, all cell culture consumables were purchased from Lonza (Verviers, Belgium).

Cell experiments

After seeding into T25 flasks, cultures were left for 24 hours to allow cells to attach and enter into S phase. After 24 hours, cells were treated with single agents: PBDE 47, PBDE 99, PBDE 153 or PCB 153 at concentrations of 10^{-8} M, 10^{-10} M or 10^{-12} M, by adding 25 µl of the appropriate treatment to each flask; vehicle controls were treated with 25 µl of DMSO (with nonane). Cells were exposed to treatments for 24 hours before they were disaggregated with trypsin, washed three times with 70% ethanol to remove residual media and then fixed for 24 hours in 70% ethanol. After fixation, cells were pipetted onto IR-reflective low-E glass slides (Kevley Technologies, Chesterland, OH, USA) and allowed to air dry before being placed in a desiccator for 24 hours to remove any remaining water. This experimental procedure was repeated at five different points in time over a 12-month period to give five technical replicates (n=5).

ATR-FTIR spectroscopy

Five spectra per slide were acquired using a Bruker TENSOR 27 FTIR spectrometer with Helios ATR attachment which contained a diamond IRE with a sampling area of 250 µm × 250 µm (Bruker Optics, Coventry, UK). Spectra were acquired with an 8 cm^{-1} spectral resolution with 32 co-additions, giving rise to a 3.84 cm^{-1} spectral data spacing. A mirror velocity of 2.2 kHz was used. Before each sample, a background measurement was taken to account for atmospheric changes and the diamond was cleaned with distilled water between samples.

Spectral pre-processing and computational analysis

An in-house Matlab 2013a (The Maths Works, MA, USA) toolbox called IRootLab was used for pre-processing and computational analysis of the spectra (http://trevisanj.github.io/irootlab/). Raw spectra were cut to 900-1800 cm^{-1}, which is known as the fingerprint region where most biomolecules are known to absorb IR. For biochemical analysis of the derivative spectra after cutting, spectra were Savitzky-Golay 2nd order differentiated (2nd order polynomial, 9 coefficients) to correct baseline aberrations and to resolve overlapping peaks. For cell comparison of exposure to single agents, spectra were baseline corrected using 1st order differentiation, vector normalised and mean-centred. Principal component analysis (PCA) was paired with linear discriminant analysis (LDA) to allow exploratory analysis of treatment-induced spectral alterations. PCA was used for data reduction purposes and was optimised, to incorporate the maximum amount of variance (~95%) whilst minimising noise incorporated into LDA, using the PCA pareto tool. LDA is a supervised technique that was used to optimise inter-class separation. K-fold (where k =5), leave-one-out cross-calculation was used to avoid overfitting. Forward feature selection was also used to compare and classify cell types. It was performed using a Gaussian fit classifier on five features using 100 randomised repeats with random subsampling. Significance of analysis results was determined in GraphPad Prism 4 (GraphPad Software Inc., CA, USA). Differences between scores from the two cell types were analysed by two-way *t*-test and differences from control in dose response scores were analysed by one-way ANOVA with Dunnett's post-hoc test. Significance testing was performed using replicate means rather than all spectral data to avoid pseudoreplication.

Nile red staining

Untreated MCF-7 and Mallard fibroblast cells were stained with Nile Red to visualise cellular lipids. Nile Red stain was purchased as a powder (Sigma-Aldrich) and made up to a 1 mg/mL stock solution, which was stored in the dark at -4˚C until use. For staining, a 1:1000 working solution was made up from the stock using PBS. Cells were snap frozen by submerging in liquid nitrogen for 30 seconds before incubation for 30 minutes in 5 mL of stain. Once stained, cells were washed twice in ice-cold PBS and air-dried. Samples were imaged by confocal microscopy using a Leica DMIRE2 inverted microscope with a Leica TCS SP2 scan head. Images were obtained using a Leica HC PL Fluotar 20× objective and a numerical aperture of 0.5.

Western blotting

For Western blot experiments, cells were seeded in 6-well culture plates at a density of 1 × 10^6 cells and allowed to grow for 24 hours before being exposed to the highest concentration of chemical treatment (10^{-8} M) for 24 hours in the same manner as described for cell experiments. Cells were lysed in 300 µl of RIPA buffer (50 mM Tris, 150 mM NaCl with 0.5% sodium deoxycholate, 1% IGEPAL CA-630 and 0.1% SDS) supplemented with protease and phosphatase inhibitor cocktails (Sigma-Aldrich). Lysates were spun at 12,000 rpm for 10 minutes and the supernatant was transferred into a clean, labelled tube. Samples were mixed 1:3 with 4× Laemmli sample buffer (containing 10% β-mercaptoethanol) and heated for 2 minutes at 95˚C. Once cooled, samples were run in a 12% acrylamide gel for 35 minutes at 180 V. Proteins were then transferred to a nitrocellulose membrane using a Bio-Rad Trans-Blot Turbo Transfer system. Membranes were blocked in a 3% solution of non-fat milk powder in Tris-buffered saline Tween-20 (TBST) for 1 hour at room temperature with constant shaking. Membranes were

then incubated with rabbit anti-CYP1A1 antibody (Abcam, Cambridge, UK), at a concentration of 1:1000, overnight at 4˚C. The membranes were washed three times in TBST before incubating, at room temperature for 1 hour, with goat anti-rabbit horseradish peroxidase-conjugated secondary antibody (Santa Cruz, CA, USA) diluted 1:10,000 in TBST. Finally, membranes were washed three times in TBTS and protein bands were quantified using Clarity Western ELC substrate on the Bio-Rad ChemiDoc XRS imaging system with β-actin as a loading control. This procedure was repeated at three different points to give three replicates (n=3). Unless stated otherwise, Western blotting related equipment and consumables were from Bio-Rad (Hercules, CA, USA).

RESULTS AND DISCUSSION

Comparison of untreated cells

In order to understand the fundamental differences between MCF-7 and Mallard cells in the absence of chemical exposures, the spectra from untreated cells were compared. The second derivatives of ATR-FTIR spectra were utilised to eliminate baseline irregularities and to resolve overlapping bands, which are particularly common in the fingerprint region (900-1800 cm^{-1}) of the spectrum. Second order differentiation results in negative facing bands where the peak maxima are at the same wavenumber as the original, undifferentiated bands. This technique is extremely useful for revealing the basic biochemistry of samples, which are subject to IR spectroscopy. Fig. 1 shows the 2nd derivative spectra of untreated MCF-7 and Mallard cells with the ten largest peaks highlighted by peak wavenumber [tentative wavenumber assignments are found in electronic supplementary information (ESI) Table 1). There are some areas of the spectrum with key peaks, which are common to both cell types. Most of these peaks are related to structure-associated macromolecules that are conserved between cell types, such as proteins.

For example, both cell spectra have a peak at 1690 cm^{-1}, which is associated with the Amide I moiety of proteins, in particular β-sheet structure vibrations. Both 2nd derivative spectra have peaks at 1512 cm^{-1} due to Amide II and in-plane CH bending and at 1393 cm^{-1} due to symmetric CH_3 bending in proteins. There are also some peaks, seen in both the MCF-7 and Mallard cell spectra, which are related to the same biomolecular vibrations but are shifted by a few wavenumbers. The peak associated with deformation of CH_3 groups in proteins is observed at 1447 cm^{-1} in MCF-7 cells but at 1450 cm^{-1} in Mallard cells. Similarly, an Amide III protein peak is visible at 1234 cm^{-1} in the MCF-7 cell spectra and 1238 cm^{-1} in the Mallard cell spectra and the peak related to C-O stretching of proteins is seen at 1165 cm^{-1} in MCF-7 cells and 1161 cm^{-1} in Mallard cells. There is also a large peak between 1600-1700 cm^{-1} present in the spectra of both cell types, which represents the largest biomolecular contribution. In both cell spectra, it appears to be composed of two bands as there are two peaks visible but the absorbance of the peaks varies with cell type. In the MCF-7 cell 2nd derivative spectra, the peak is found at 1624 cm^{-1} and in the Mallard cell spectrum, it is found at 1639 cm^{-1}. This may be due to slightly different vibrational modes of Amide I molecules due to varying types and proportions proteins [26] or due to differences in the secondary structure of proteins which can be reflected in small shifts in the Amide I band in derivative spectra [27].

Possibly of more interest, there are also regions of the spectrum, which are distinctly different in MCF-7 and Mallard cells. In the Mallard cell spectrum, this is mainly due to the peak at 1744 cm^{-1} which is associated with C=O stretching of lipids and triglycerides. This peak is almost non-existent in the MCF-7 cell spectrum indicating that there is more intracellular lipid in Mallard cells. This may be due to the nature of the Mallard cells, which are fibroblasts derived from the skin. The avian epidermis has unique subkeratinocytes which produce lipids needed to

keep the skin and feathers healthy [28]. This could represent an important modification seen in some avian cells and may have implication for how susceptible certain cell types are to exposure to contaminants. Dermal contact may be an important exposure route [29] and additionally, many environmental contaminants are lipophilic and may be able to sequester easier in Mallard cells [30]. There is also a unique peak in the Mallard spectrum at 1312 cm^{-1} related to Amide III vibrations. Another peak, seen at 1080 cm^{-1} in Mallard cells, is due to symmetric phosphate stretching vibrations in nucleic acids and although the 1084 cm^{-1} peak in the MCF-7 spectrum is also associated with this, the peak at 1080 cm^{-1} has also been linked to collagen presence. This may also be due to the Mallard fibroblast cells originating from the skin which is known to contain collagen [31]. In the MCF-7 cell 2nd derivative spectrum, there are two unique peaks at 1057 cm^{-1} and 964 cm^{-1}, which are related to C-C or C-O stretching of deoxyribose in DNA. MCF-7 cells are epithelial cells from a mammary tumour and thus may have different DNA characteristics as a higher proportion of cells are likely to be in the S and G_2 growth phases [32]. MCF-7 cells also have a doubling time of 29 hours whereas avian cells are generally slower growing as birds are often longer lived than mammals of the same size [25]. The Mallard fibroblasts had a doubling time of ~48 hours.

Using multivariate analysis, PCA-LDA was also used to explore and visualise the differences and similarities between the two cell types. Fig. 2A and 2B shows the one-dimensional (1D) scores plots and corresponding loadings from this analysis. The scores plots indicate that untreated MCF-7 and Mallard cells are significantly different (P<0.01) along the LD1 axis. Co-clustering and lack of overlap of scores along LD1 signifies that there is variation between the two cell types as in these types of plots, dissimilarity is indicated by increasing distance [8]. The loadings (Fig. 2B) display the absorbances of biomolecules that are responsible

for the separation seen in the scores plot; the six largest peaks representing the most contributing wavenumbers have been highlighted with tentative assignments (Fig. 2D). Some of the wavenumbers in the loadings reflect the main peaks seen in the 2nd derivative spectra (Fig. 1) including the peak at 1740 cm^{-1} which is associated with C=O stretching of lipids and the deoxyribose peak at 964 cm^{-1}. Additionally there are peaks in the loadings at 1717 cm^{-1} and 1485 cm^{-1} due to nucleic acids (thymine and guanine respectively) which may be related to DNA differences seen in MCF-7 cells in the derivative spectra. There is also a lipid-related peak at 1416 cm^{-1} which as previously established, may be due to differences in cellular lipid profiles. The other peaks seen in the loadings are associated with protein variation; 1694 cm^{-1} (Amide I) and 1512 cm^{-1} (Amide II). To further explore the biochemical differences which discriminate the cell types and to validate that the ATR-FTIR spectrochemical technique is able to distinguish between them, forward feature selection (FFS) was employed as well as PCA-LDA. FFS ranks subsets of wavenumbers based on how much they contribute to the classification of the spectra into the experimental groups [27]. A classification rate of 100% was achieved and the feature histogram seen in Fig. 2C shows the top six wavenumbers which had the most hits when cells were classified (assignments found in Fig. 2D). This confirms that the wavenumbers responsible for discriminating between MCF-7 and Mallard cells are largely associated with lipid content. Two of the features with the most hits are observed at 1790 cm^{-1} and 1755 cm^{-1} which are both associated with vibrations of C=C bonds in lipids and fatty acids. The other features highlighted are mostly related to the protein content of the cells, which is mirrored in the loadings and 2nd derivative spectra. The other peaks in the feature histogram can be seen at 1697 cm^{-1} (Amide I), 1639 cm^{-1} (Amide I), 1520 cm^{-1} (Amide II and CH bending) and 1161 cm^{-1} (C-O vibrations from proteins).

As cellular lipid content emerged as a consistent discriminatory feature in the analysis, the cells were stained with Nile red stain and imaged using confocal microscopy (Fig. 3). Nile red is a vital stain which is highly soluble in lipids and is strongly fluorescent but only in the presence of a hydrophobic, lipid-rich environment [33]. It is visually obvious that the staining pattern in the two cell lines differs suggesting that MCF-7 and Mallard cells have dissimilar intracellular lipid distribution. In MCF-7 cells, lipids appear to be mostly accumulated around the periphery of the cells indicating that most of the lipid is found in the cell membrane. However in the Mallard cells, lipids appear to be distributed throughout the cytoplasm so that the cell membrane cannot be distinguished. The nucleus is visualised as a 'hole' in the staining as less lipid is localised there. As previously suggested, the difference in lipid distribution is likely due to increased lipid content in bird skin cells, including Mallards. Although this will not be a feature of all avian cell types, because such a lipid profile may provide an ideal environment for the accumulation of lipophilic chemicals it could have implications for extrapolation of results from toxicity tests using traditional cell line assays. As the cells are very different in physiology, lipidomic analysis to provide quantitative lipid values for the two cells types should be performed to confirm this. Another reoccurring feature was wavenumbers related to DNA and nucleic acid molecules in the cells, possibly as the MCF-7 cells are from a breast cancer cell line with altered gene expression patterns. MCF-7 cells have been found to express higher basal levels of cytochrome P450 enzymes compared to benign epithelium and exhibit an increased inducible response to contaminant exposure and at basal levels compared to normal epithelial cells [34]; hence a Western blot was performed to assess CYP1A1 levels in the absence of treatment (see ESI Fig. 1). It appeared that basal expression of CYP1A1 in Mallard cells was almost half that observed in MCF-7 cells, which may indicate that metabolism of xenobiotic

compounds is likely to be different. Previous work has found that MCF-7 cells preferentially express CYP1A1 [35] whereas in avian species, other isoforms such as CYP1A4 or CYP1A5 may be more important [36]. However, it is important to recognise that whilst some Mallard isoforms are orthologous to mammalian CYP1A1, the degree of homology is not perfect which could interfere with the efficacy of antibody-based assays [37]. Therefore, cytochrome P450 metabolism differences cannot be determined with certainty until the strength of avian CYP isoforms binding to CYP antibodies has been fully validated. This would also need to be fully tested in response to a number of different compounds and to investigate their consequent effects on different CYP isoforms, all which may have implications for species-based susceptibility to contaminants.

Exposure to PCB and PBDE congeners

IR spectroscopy is a powerful tool that not only allows insight into the underlying biochemical structure of samples but can also be applied to reveal the effects of chemical treatments by extracting induced spectral alterations. In order to see if differences in biochemistry influence the effects on MCF-7 and Mallard cells when exposed to single PCB or PBDE agents, the PCA-LDA processed spectral datasets were visualised as 1D scores plots with corresponding loadings from LD1. Scores plots of both cells treated with 10^{-8} M, 10^{-10} M or 10^{-12} M PBDE 47 (Fig. 4, see ESI Table 2) show that all cells exposed to the chemical segregate significantly (P<0.01) away from the controls. This suggests that treatment with PBDE 47 at these concentrations induces significant biochemical changes in both human and avian cells. The major wavenumber assigned alterations that contribute to this separation in Mallard cells are in spectral regions associated with lipids (1767 cm^{-1}; 1713 cm^{-1}), C=O stretching of Amide I (1643 cm^{-1}), Amide II (1543 cm^{-1}; 1497 cm^{-1}) and protein CH_3 deformation (1454 cm^{-1}). In MCF-7

cells, treatment with PBDE 47 is associated with fatty acids (1724 cm^{-1}), Amide I (1636 cm^{-1}), Amide II (1555 cm^{-1}; 1520 cm^{-1}), asymmetric phosphate stretching vibrations in DNA (1219 cm^{-1}) and glycogen and ribose vibrations (1030 cm^{-1}). Both cell types exhibit alterations in the lipid region of the spectrum in response to PBDE 47 exposure. In both loadings plots, two peaks with the same direction and similar magnitudes of change can be seen in the lipid region between 1751 and 1771 cm^{-1}. This suggests that PBDE47 induces similar effects on both cell types in this region of the spectrum. In Mallard cells, the lipid alteration associated peaks are among the largest changes induced by the chemical whereas in MCF-7 cells, these alterations are surpassed in magnitude by those associated protein and DNA. The two cell types exhibit a different range of biomarkers of exposure to PBDE 47 with alterations in Mallard cells occurring in lipid and protein regions and MCF-7 cell alterations occurring in lipid, protein, DNA and carbohydrate regions. The unique DNA alterations in MCF-7 cell spectra may reflect an essential difference in cellular biochemistry between the two cell types. As seen in Fig. 5 (and ESI Table 3), similar alteration profiles appear to be seen in MCF-7 cells when exposed to PBDE 99 and those treated with PBDE 47. MCF-7 cells treated with PBDE 99 showed alterations in peaks of lipids and fatty acids (1755 cm^{-1}), C=O vibration of Amide I (1632 cm^{-1}), Amide II (1578 cm^{-1};1400 cm^{-1}), symmetric phosphate stretching vibrations in DNA (1076 cm^{-1}) and collagen (1034 cm^{-1}). However, it is important to note that there was considerable overlap of the scores from PBDE 99-treated MCF-7 cells with the control, resulting in an insignificant result and this limits the conclusions that can be drawn from the loadings. Visually similar loadings profiles could suggest similar profiles of exposure induced by these congeners but this would need further investigation to be conclusive. In avian cells, exposure was characterised by extensive alterations in lipid and protein associated spectral regions. The major alterations were seen in C=C and C=O bonds of

lipid molecules (1748 cm^{-1}; 1713 cm^{-1}), C=O, C-N or N-H bond vibrations of Amide I (1655 cm^{-1}) and Amide II (1597 cm^{-1}; 1555 cm^{-1}; 1504 cm^{-1}). The major wavenumber-associated alterations from PBDE 153-treated MCF-7 cells (Fig. 6, see ESI Table 4) are seen in Amide I (1697 cm-1; 1651 cm^{-1}) and Amide II (1539 cm^{-1}; 1504 cm^{-1}) groups from proteins as well as carbohydrates including glycogen (1049 cm^{-1}) and DNA phosphodiester stretching (903 cm^{-1}). PBDE 153 treatment induced MCF-7 cell specific alterations in carbohydrates and DNA spectral regions that are not seen in Mallard cells treated with this chemical. However, alterations induced in Mallard cells by PBDE 153 exposure are not explored here as the scores were not significantly separated except at a concentration of 10^{-12} M. This means that the loadings cannot be interpreted with accuracy as they will also incorporate potentially meaningless biological information from unseparated scores. Finally, alterations in MCF-7 and Mallard cells treated with 10^{-8} M, 10^{-10} M or 10^{-12} M of PCB 153 can be seen in Fig. 7, see ESI Table 5. After exposure, MCF-7 cells were characterised by changes in fatty acid esters (1732 cm^{-1}), Amide I (1697 cm^{-1}; 1643 cm^{-1}), Amide II (1543 cm^{-1}; 1597 cm^{-1}) and symmetric phosphate stretching vibrations of DNA (1072 cm^{-1}) whereas Mallard cells exposed to PCB 153 exhibited alterations in lipids (1709 cm^{-1}), Amide I (1694 cm^{-1}), Amide II (1535 cm^{-1}; 1497 cm^{-1}) and other structural and functional molecules including collagen and glycogen (1458 cm^{-1} and 1030 cm^{-1}, respectively) in avian cells.

Overall, spectra from both cell types treated with PBDE 47, PBDE 99, PBDE 153 or PCB 153 show alterations mostly in Amide I and II protein regions, with unique DNA alterations seen in MCF-7 spectra. Alterations in lipid-associated spectral regions were also seen in both cell types, particularly in response to PBDE 47 and PCB 153 exposures. This is consistent with what we know of these types of chemicals and the cellular changes they can stimulate. PCBs and

PBDEs can induce a number of cellular effects which could cause alterations in protein in both cell types, such as induction of enzymes involved in phase I and II xenobiotic metabolism and changes to regulatory or structural proteins [38]. They are also lipophilic chemicals and have been shown to cause a range of toxic effects which can cause cellular lipid alterations including instigating oxidative stress and lipid peroxidation [39]. Lipid alterations were amongst the most marked induced in Mallard cells by all congeners which may indicate that they are susceptible to lipophilic compounds such as PCBs and PBDEs, that can alter lipid metabolism [40] and production of ROS leading to lipid damage [39]. This may be due to lipid distribution throughout this cell type, which appears to be throughout the cytoplasm as seen in Nile red-stained images. Other cell types have been found to be differentially affected by certain contaminants due to their lipid content, for example neurons with myelin sheaths are thought to be susceptible to organochlorine chemicals [41]. Untreated MCF-7 cells were found to exhibit more spectral contributions from DNA than Mallard cells and correspondingly, more DNA alterations were induced by exposure to PCB and PBDE contaminants in these cells than in their avian counterparts. Both PCBs and PBDEs can damage DNA either directly or by producing free-radicals and causing oxidative stress [42]-[43, 44] and thus the native biochemical differences of MCF-7 cells may make them more susceptible to this type of toxicity. This could potentially lead to an over-estimation of toxic risk in cell-based assays using MCF-7 cells. Therefore, for cell-based toxicity testing, it may be appropriate to use a number of representative cell types to ensure accurate results. As this could potentially be time-consuming and costly, ATR-FTIR spectroscopy may have a novel application as a tool to rapidly screen multiple cell lines [45] in order to determine which cell types are differentially affected by a treatment before full toxicity testing is performed.

As with many preliminary exploratory studies, there are weaknesses in this work, which can be used to direct and improve future experiments. The concentrations used in this study were selected to simulate exposure levels of contaminants that would be encountered by organisms in the environment, particularly as one of the cell lines used is derived from a free-flying duck species. Previous work has identified spectral protein and lipid alterations in MCF-7 cells at concentrations as low as 10^{-12} M due to bimodal dose responses [23] but the majority of studies focus on concentrations above the μM range [46]. The Mallard cell line appears to respond differently to dose response experiments than the MCF-7 cells. Therefore, some of the results are not significant particularly at lower concentrations, which limits conclusions that can be made. In order to avoid this, future experiments should focus on concentrations above the μM range before investigating the response of cells at very low environmental levels. With the use of such small concentrations, the measurement of other sub-lethal toxicological effect markers would be also useful. This may also increase the stability of the PCA-LDA models and allow dose-response scores clusters to be consistently resolved. The results presented here were analysed using PCA-LDA as the results from PCA were not found to be significant (see ESI Figs. 2-5, Table 6).

The results from this initial spectral study indicate that MCF-7 and Mallard cells have unique biochemical differences and the results of studies like this can contribute to important decisions regarding which cell types should be used in toxicology assays. This may be particularly essential when studying environmental contaminants and want to extrapolate the results to environmental species. Biochemical differences, which can be identified using ATR-FTIR spectroscopic techniques, may influence how cell types used in assays are affected by common environmental contaminants such as PCBs and PBDEs. This study demonstrates ATR-

FTIR spectroscopy as an exploratory tool to investigate biochemical differences at the cellular level and may have practical application as a means to direct further work. Such techniques could be used as part of a panel of cell-based assays to indicate when results from environmentally derived cell lines differ from those obtained from traditional cell lines, which might vastly differ in many aspects, *e.g.*, metabolism, biochemistry etc. This is a preliminary study and future work is needed to understand where and how Mallard fibroblast cells and other environmental cell lines can be used but with optimisation the use of IR spectroscopy to analyse environmentally relevant cell lines could improve the extrapolation of results to environmental settings in a cost and time efficient manner.

CONCLUSIONS

Differences at the molecular, cellular, tissue and/or species level can affect the toxicity of environmental chemical contaminants. Cell-based assays to investigate the toxicity of such compounds are highly useful in the effort to reduce the number of animals used in scientific procedures but appropriate cell types must be used in order to obtain meaningful results. To investigate environmentally relevant chemicals, a cell line closer to those found in the environment may be more suitable for extrapolation of results. By using ATR-FTIR spectroscopy to analyse untreated cells, the spectra of an MCF-7 and a Mallard fibroblast cell line were compared to understand cellular differences, which might affect the results of cell-based toxicity testing. The two cell types were found to share some spectral features, in the fingerprint region, largely due to cellular macromolecules such as proteins. However, each cell type spectrum also demonstrated unique differences in biochemical composition. Untreated Mallard cell spectra displayed large lipid-associated peaks, possibly due to greater intracellular lipid content, which was explored in Nile red-stained images. MCF-7 cells were found to have

spectral differences in the DNA and nucleic acid regions, possibly as the cell line is derived from an epithelial breast tumour. This demonstrates that ATR-FTIR spectroscopy can identify fundamental biochemical cellular differences. It is possible that these biochemical differences may also determine how environmental pollutants will affect cells and thus could influence how accurate the extrapolation of toxicity test results to environmental species will be. However, further characterisation of Mallard fibroblasts would be needed. Differences in the biomolecular structure and composition of cells must be considered during such testing and if possible, multiple cell types should be analysed. ATR-FTIR with multivariate analysis can be used as a powerful tool for this purpose as it can be used to discriminate between cell types based on fundamental variances at the biomolecular level. This technique may be particularly useful as a screening tool to analyse variations in response to chemical exposure before full toxicology testing is performed. In this manner, ATR-FTIR spectroscopy would allow researchers to obtain rapid initial findings that can direct conclusive toxicological investigation. It is not possible to say from this initial study whether Mallard fibroblasts are the most suitable environmental 'surrogate' for toxicology tests using mammalian cells so future work would focus on additional characterisation of Mallard fibroblasts as well as investigation of cellular differences in cell lines from other environmental species such as amphibians and fish.

Supplemental Data—The Supplemental Data are available on the Wiley Online Library at DOI: 10.1002/etc.xxxx.

Acknowledgment—The authors wish to thank J. M. Harper of Sam Houston State University who generously provided the Mallard fibroblast cells. K.H. is a NERC-CEH funded PhD student.

Data availability—Data, associated metadata, and calculation tools are available from the corresponding author (flmartin@uclan.ac.uk).

REFERENCES

1. De Zwart D, Posthuma L. 2005. Complex mixture toxicity for single and multiple species: proposed methodologies. *Environmental Toxicology and Chemistry* 24:2665-2676.

2. Walker CH, Sibly R, Hopkin S, Peakall DB. 2012. *Principles of ecotoxicology*. CRC press.

3. Liu Y, Vijver MG, Qiu H, Baas J, Peijnenburg WJ. 2015. Statistically significant deviations from additivity: What do they mean in assessing toxicity of mixtures? *Ecotoxicology and environmental safety* 122:37-44.

4. Kazarian SG, Chan KA. 2013. ATR-FTIR spectroscopic imaging: recent advances and applications to biological systems. *Analyst* 138:1940-1951.

5. Chen Y, Zou C, Mastalerz M, Hu S, Gasaway C, Tao X. 2015. Applications of Micro-Fourier Transform Infrared Spectroscopy (FTIR) in the Geological Sciences—A Review. *International journal of molecular sciences* 16:30223-30250.

6. Butler HJ, McAinsh MR, Adams S, Martin FL. 2015. Application of vibrational spectroscopy techniques to non-destructively monitor plant health and development. *Analytical Methods* 7:4059-4070.

7. Obinaju BE, Alaoma A, Martin FL. 2014. Novel sensor technologies towards environmental health monitoring in urban environments: A case study in the Niger Delta (Nigeria). *Environmental Pollution* 192:222-231.

8. Kelly JG, Trevisan J, Scott AD, Carmichael PL, Pollock HM, Martin-Hirsch PL, Martin FL. 2011. Biospectroscopy to metabolically profile biomolecular structure: a multistage approach linking computational analysis with biomarkers. *Journal of proteome research* 10:1437-1448.

9. Martin FL, Kelly JG, Llabjani V, Martin-Hirsch PL, Patel II, Trevisan J, Fullwood NJ, Walsh MJ. 2010. Distinguishing cell types or populations based on the computational analysis of their infrared spectra. *Nature protocols* 5:1748-1760.

10. Llabjani V, Crosse JD, Ahmadzai AA, Patel II, Pang W, Trevisan J, Jones KC, Shore RF, Martin FL. 2011. Differential effects in mammalian cells induced by chemical mixtures in environmental biota as profiled using infrared spectroscopy. *Environmental science & technology* 45:10706-10712.

11. Strong RJ, Halsall CJ, Jones KC, Shore RF, Martin FL. 2016. Infrared spectroscopy detects changes in an amphibian cell line induced by fungicides: Comparison of single and mixture effects. *Aquatic Toxicology* 178:8-18.

12. Riding MJ, Martin FL, Trevisan J, Llabjani V, Patel II, Jones KC, Semple KT. 2012. Concentration-dependent effects of carbon nanoparticles in gram-negative bacteria determined by infrared spectroscopy with multivariate analysis. *Environmental pollution* 163:226-234.

13. Obinaju BE, Graf C, Halsall C, Martin FL. 2015. Linking biochemical perturbations in tissues of the African catfish to the presence of polycyclic aromatic hydrocarbons in Ovia River, Niger Delta region. *Environmental Pollution* 201:42-49.

14. Jeon Y, Sung J, Kim D, Seo C, Cheong H, Ouchi Y, Ozawa R, Hamaguchi H-o. 2008. Structural change of 1-butyl-3-methylimidazolium tetrafluoroborate+ water mixtures studied by infrared vibrational spectroscopy. *The Journal of Physical Chemistry B* 112:923-928.

15. Ewing AV, Gabrienko AA, Semikolenov SV, Dubkov KA, Kazarian SG. 2014. How Do Intermolecular Interactions Affect Swelling of Polyketones with a Differing Number of Carbonyl Groups? An In Situ ATR-FTIR Spectroscopic Study of CO2 Sorption in Polymers. *The Journal of Physical Chemistry C* 119:431-440.

16. Llabjani V, Trevisan J, Jones KC, Shore RF, Martin FL. 2010. Binary mixture effects by PBDE congeners (47, 153, 183, or 209) and PCB congeners (126 or 153) in MCF-7 cells: biochemical alterations assessed by IR spectroscopy and multivariate analysis. *Environmental science & technology* 44:3992-3998.

17. Baker MJ, Trevisan J, Bassan P, Bhargava R, Butler HJ, Dorling KM, Fielden PR, Fogarty SW, Fullwood NJ, Heys KA, Hughes C, Lasch P, Martin-Hirsch PL, Obinaju B, Sockalingum GD, Sulé-Suso J, Strong RJ, Walsh MJ, Wood BR, Gardner P, Martin FL. 2014. Using Fourier transform IR spectroscopy to analyze biological materials. *Nature protocols* 9:1771-1791.

18. Stephens ML. 2010. An animal protection perspective on 21st century toxicology. *Journal of Toxicology and Environmental Health, Part B* 13:291-298.

19. Scholz S, Sela E, Blaha L, Braunbeck T, Galay-Burgos M, Garcia-Franco M, Guinea J, Kluever N, Schirmer K, Tanneberger K. 2013. A European perspective on alternatives to animal testing for environmental hazard identification and risk assessment. *Regulatory toxicology and pharmacology* 67:506-530.

20. Huang X, Chen L, Liu W, Qiao Q, Wu K, Wen J, Huang C, Tang R, Zhang X. 2015. Involvement of oxidative stress and cytoskeletal disruption in microcystin-induced apoptosis in CIK cells. *Aquatic Toxicology* 165:41-50.

21. Leist M, Hasiwa N, Daneshian M, Hartung T. 2012. Validation and quality control of replacement alternatives–current status and future challenges. *Toxicology Research* 1:8-22.

22. Bols N, Dayeh V, Lee L, Schirmer K. 2005. Use of fish cell lines in the toxicology and ecotoxicology of fish. Piscine cell lines in environmental toxicology. *Biochemistry and molecular biology of fishes* 6:43-84.

23. Barber JL, Walsh MJ, Hewitt R, Jones KC, Martin FL. 2006. Low-dose treatment with polybrominated diphenyl ethers (PBDEs) induce altered characteristics in MCF-7 cells. *Mutagenesis* 21:351-360.

24. Li J, Strong R, Trevisan J, Fogarty SW, Fullwood NJ, Jones KC, Martin FL. 2013. Dose-related alterations of carbon nanoparticles in mammalian cells detected using biospectroscopy: potential for real-world effects. *Environmental science & technology* 47:10005-10011.

25. Harper JM, Wang M, Galecki AT, Ro J, Williams JB, Miller RA. 2011. Fibroblasts from long-lived bird species are resistant to multiple forms of stress. *Journal of Experimental Biology* 214:1902-1910.

26. de Campos Vidal B, Mello MLS. 2011. Collagen type I amide I band infrared spectroscopy. *Micron* 42:283-289.

27. Gallagher W. 2009. FTIR analysis of protein structure. *Course manual Chem* 455.

28. Menon GK, Menon J. 2000. Avian epidermal lipids: functional considerations and relationship to feathering. *American Zoologist* 40:540-552.

29. Shore RF, Taggart MA, Smits J, Mateo R, Richards NL, Fryday S. 2014. Detection and drivers of exposure and effects of pharmaceuticals in higher vertebrates. *Phil Trans R Soc B* 369:20130570.

30. Arts MT, Brett MT, Kainz M. 2009. *Lipids in aquatic ecosystems*. Springer Science & Business Media.

31. Prum RO, Torres R. 2003. Structural colouration of avian skin: convergent evolution of coherently scattering dermal collagen arrays. *Journal of Experimental Biology* 206:2409-2429.

32. Hammiche A, German MJ, Hewitt R, Pollock HM, Martin FL. 2005. Monitoring cell cycle distributions in MCF-7 cells using near-field photothermal microspectroscopy. *Biophysical journal* 88:3699-3706.

33. Greenspan P, Mayer EP, Fowler SD. 1985. Nile red: a selective fluorescent stain for intracellular lipid droplets. *The Journal of cell biology* 100:965-973.

34. Angus WG, Larsen MC, Jefcoate CR. 1999. Expression of CYP1A1 and CYP1B1 depends on cell-specific factors in human breast cancer cell lines: role of estrogen receptor status. *Carcinogenesis* 20:947-955.

35. Spink DC, Spink BC, Cao JQ, DePasquale JA, Pentecost BT, Fasco MJ, Li Y, Sutter TR. 1998. Differential expression of CYP1A1 and CYP1B1 in human breast epithelial cells and breast tumor cells. *Carcinogenesis* 19:291-298.

36. Mahajan S, Rifkind A. 1999. Transcriptional Activation of AvianCYP1A4andCYP1A5by 2, 3, 7, 8-Tetrachlorodibenzo-p-dioxin: Differences in Gene Expression and Regulation Compared to MammalianCYP1A1andCYP1A2. *Toxicology and applied pharmacology* 155:96-106.

37. Watanabe KP, Kawai YK, Ikenaka Y, Kawata M, Ikushiro S-I, Sakaki T, Ishizuka M. 2013. Avian cytochrome P450 (CYP) 1-3 family genes: isoforms, evolutionary relationships, and mRNA expression in chicken liver. *PLoS One* 8:e75689.

38. Alm H, Scholz B, Kultima K, Nilsson A, Andren PE, Savitski MM, Bergman Å, Stigson M, Fex-Svenningsen Å, Dencker L. 2009. In vitro neurotoxicity of PBDE-99: immediate and concentration-dependent effects on protein expression in cerebral cortex cells. *Journal of proteome research* 9:1226-1235.

39. He P, He W, Wang A, Xia T, Xu B, Zhang M, Chen X. 2008. PBDE-47-induced oxidative stress, DNA damage and apoptosis in primary cultured rat hippocampal neurons. *Neurotoxicology* 29:124-129.

40. Noël M, Loseto LL, Helbing CC, Veldhoen N, Dangerfield NJ, Ross PS. 2014. PCBs are associated with altered gene transcript profiles in Arctic beluga whales (Delphinapterus leucas). *Environmental science & technology* 48:2942-2951.

41. Cannon JR, Greenamyre JT. 2011. The role of environmental exposures in neurodegeneration and neurodegenerative diseases. *Toxicological Sciences*:kfr239.

42. Ravoori S, Ayotte P, Srinivasan C, Pereg D, Robertson LW, Russell GK, Jeyabalan J, Gupta RC. 2008. DNA damage associated with PCBs in the whole blood cells of Inuit. *Environmental toxicology and pharmacology* 25:273-276.

43. Schilderman P, Maas L, Pachen D, De Kok T, Kleinjans J, Van Schooten F. 2000. Induction of DNA adducts by several polychlorinated biphenyls. *Environmental and molecular mutagenesis* 36:79-86.

44. Alabi OA, Bakare AA, Xu X, Li B, Zhang Y, Huo X. 2012. Comparative evaluation of environmental contamination and DNA damage induced by electronic-waste in Nigeria and China. *Science of the Total Environment* 423:62-72.

45. Balls M, Combes RD, Bhogal N. 2012. *New Technologies for Toxicity Testing*. Springer Science & Business Media.

46. Li Z-H, Liu X-Y, Wang N, Chen J-S, Chen Y-H, Huang J-T, Su C-H, Xie F, Yu B, Chen D-J. 2012. Effects of decabrominated diphenyl ether (PBDE-209) in regulation of growth and apoptosis of breast, ovarian, and cervical cancer cells. *Environmental health perspectives* 120:541.

Figure 1. Mean ATR-FTIR 2nd derivative spectra from untreated (**A**) MCF-7 cells and (**B**) Mallard cells in the biological fingerprint region of 900-1800 cm^{-1} with the top ten peaks labelled.

Figure 2. Comparison of untreated MCF-7 and Mallard cells. (A) ATR-FTIR PCA-LDA scores plot showing separation of scores along LD1, significance assessed by two-sample *t*-test ($P<0.01$ level indicated by ** symbol); (**B**) LD1 loadings describing wavenumber alterations responsible for separation in scores plots with the top six peaks highlighted; (**C**) Forward feature selection histogram resulting from 100% classification of cell type; (**D**) Tentative wavenumber assignments, derived from Movasaghi et al, 2008.

Figure 3. Confocal microscopy images of untreated cells stained with 1:1000 Nile Red stain to show cellular lipids. Images obtained using a 20× objective and a numerical aperture of 0.5. (**A**) MCF-7 cells; (**B**) Mallard cells.

Figure 4. Comparison of ATR-FTIR PCA-LDA scores plots and corresponding loadings plots for MCF-7 and Mallard cells treated with 10^{-8}, 10^{-10} or 10^{-12} M PBDE 47. Significance from control calculated using one-way ANOVA followed by Dunnett's post-hoc test ($P<0.05$ level (*) or $P<0.01$ level (**). Arrows signify similar alterations induced in the lipid region in the range between 1751 and 1771 cm^{-1}.

Figure 5. Comparison of Comparison of ATR-FTIR PCA-LDA scores plots and corresponding loadings plots for MCF-7 and Mallard cells treated with 10^{-8}, 10^{-10} or 10^{-12} M PBDE 99. Significance from control calculated using one-way ANOVA followed by Dunnett's post-hoc test ($P<0.05$ level (*) or $P<0.01$ level (**)

Figure 6. Comparison of ATR-FTIR PCA-LDA scores plots and corresponding loadings plots from MCF-7 and Mallard cells treated with 10^{-8}, 10^{-10} or 10^{-12} M PBDE 153. Significance from

control calculated using one-way ANOVA followed by Dunnett's post-hoc test (P<0.05 level (*) or P<0.01 level (**).

Figure 7. Comparison of ATR-FTIR PCA-LDA scores plots and corresponding loadings plots from MCF-7 and Mallard cells treated with 10^{-8}, 10^{-10} or 10^{-12} M PCB 153. Significance from control calculated using one-way ANOVA followed by Dunnett's post-hoc test (P<0.05 level (*) or P<0.01 level (**).

Table 1 – Fingerprint region (900-1800 cm^{-1}) tentative wavenumber assignments from second derivative ATR-FTIR spectra of untreated MCF-7 and Mallard cells. Assignments were derived from Movasaghi et al, 2008.

Cell Type	Wavenumber (cm^{-1})	Tentative Assignment
MCF-7	1690	Amide I; nucleic acids in carbonyl base
	1624	Amide I; nucleic acids in carbonyl base
	1512	Amide II; CH bending
	1447	CH_3 vibrations from proteins
	1393	CH_3 vibrations from proteins
	1234	Amide III; nucleic acid phosphate vibrations
	1165	C-O stretching of proteins
	1084	Phosphate vibrations from DNA
	1057	C-O stretching of deoxyribose
	964	C-C and C-O of deoxyribose in DNA
Mallard	1744	C=O stretching mode of lipids and triglycerides
	1690	Amide I; nucleic acids in carbonyl base
	1639	Amide I

	1512	Amide II; CH bending
	1450	CH_3 vibrations from proteins
	1393	CH_3 vibrations from proteins
	1312	Amide III of proteins
	1238	Amide III; asymmetric phosphate stretching
	1161	C-O stretching of proteins
	1080	Symmetric phosphate stretching; Collagen

Figure 1

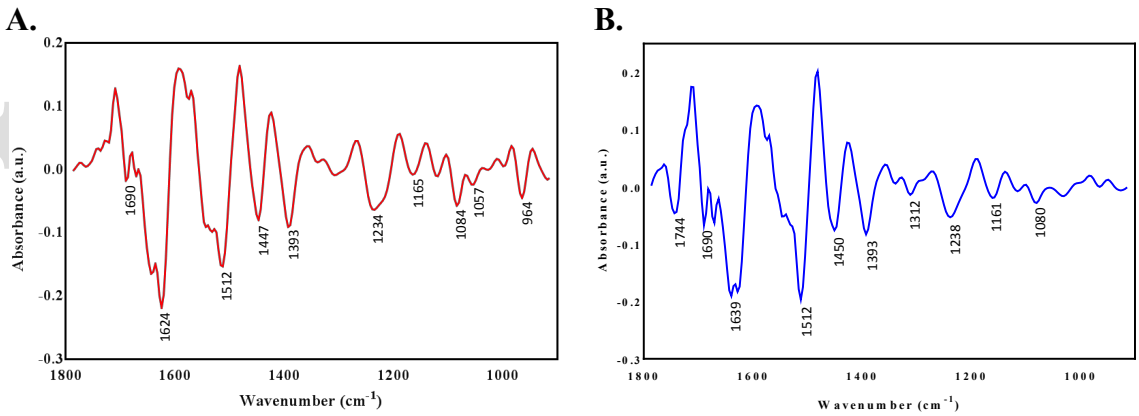

Figure 2

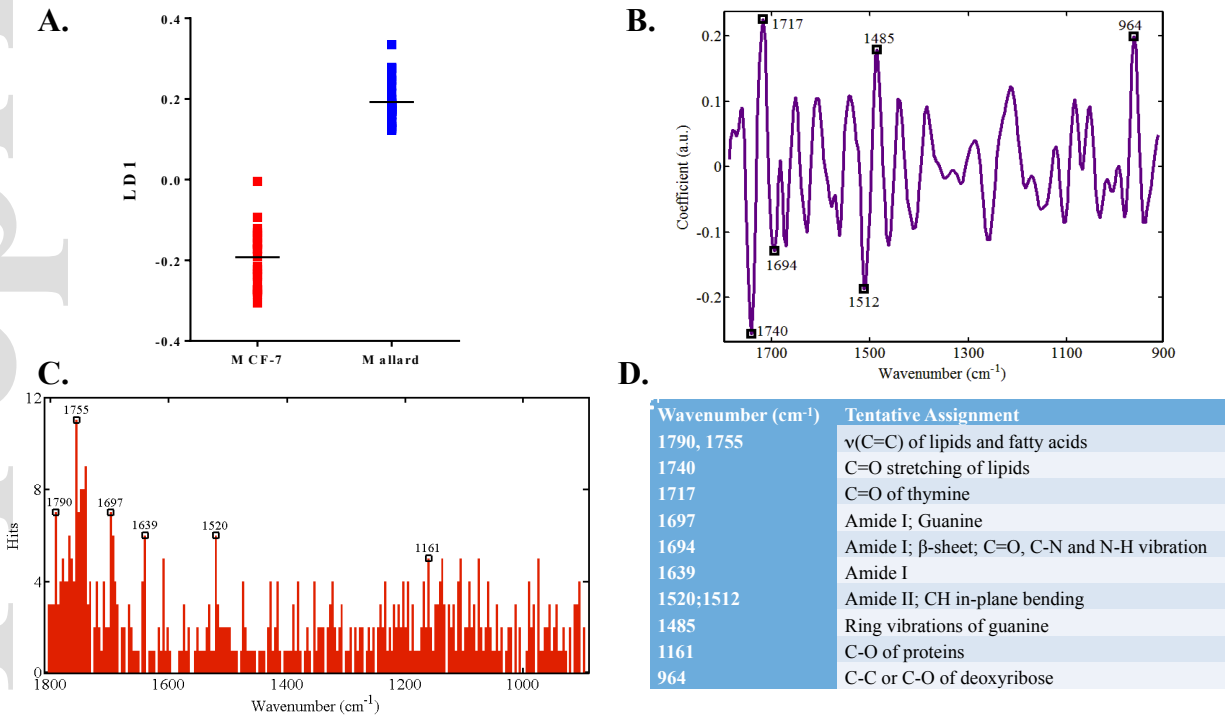

D.

Wavenumber (cm^{-1})	Tentative Assignment
1790, 1755	ν(C=C) of lipids and fatty acids
1740	C=O stretching of lipids
1717	C=O of thymine
1697	Amide I; Guanine
1694	Amide I; β-sheet; C=O, C-N and N-H vibration
1639	Amide I
1520;1512	Amide II; CH in-plane bending
1485	Ring vibrations of guanine
1161	C-O of proteins
964	C-C or C-O of deoxyribose

Figure 3

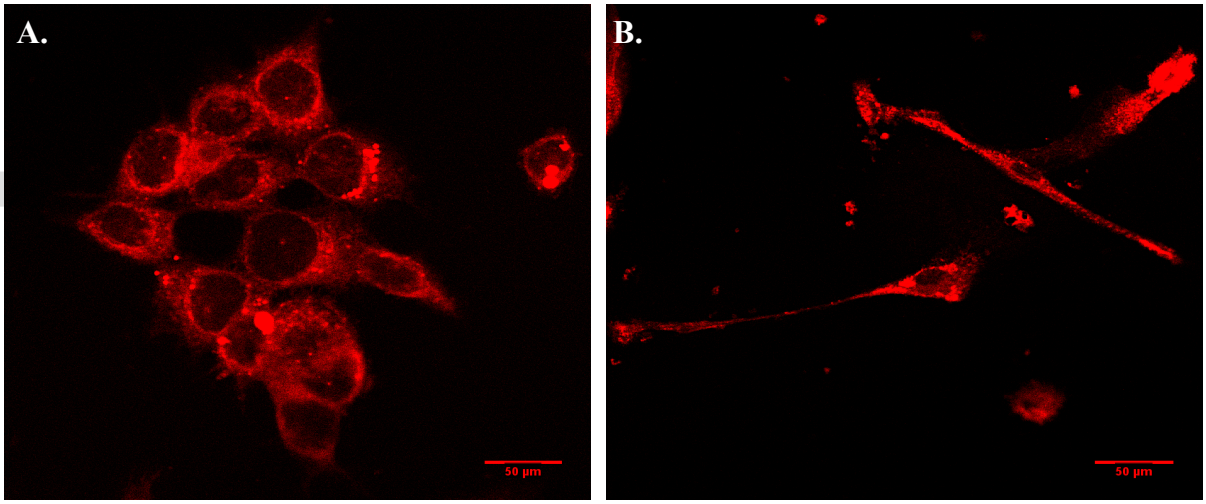

Figure 4

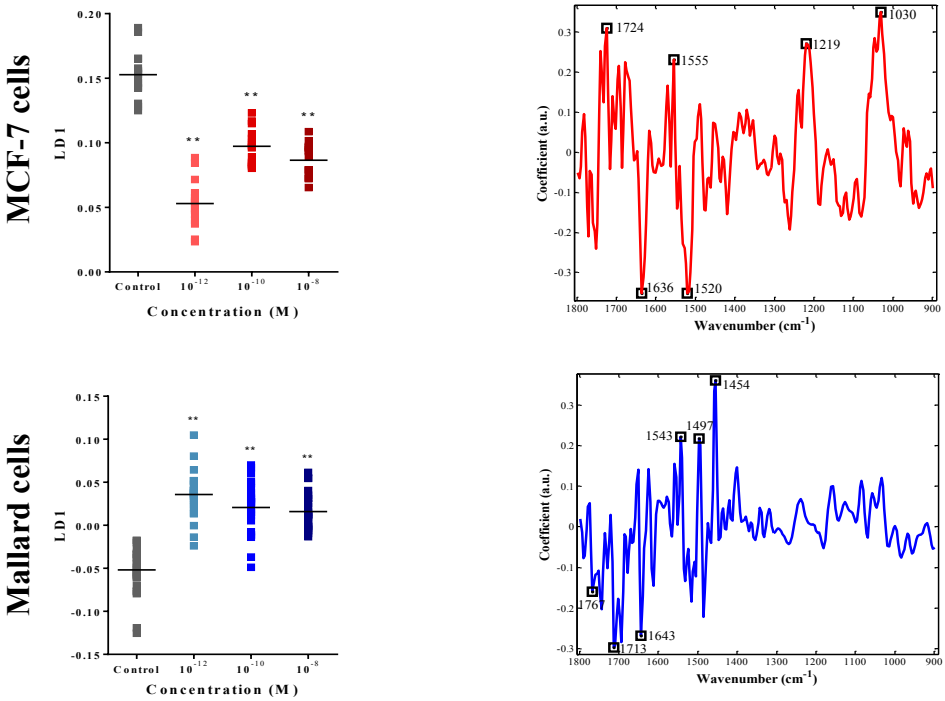

Figure 5

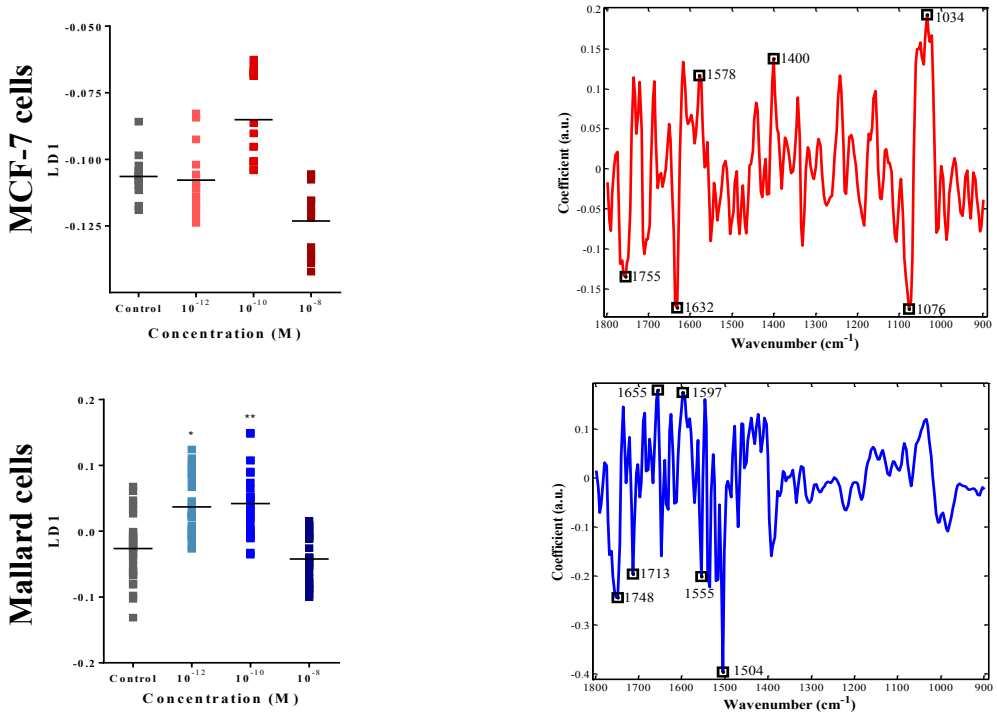

Figure 6

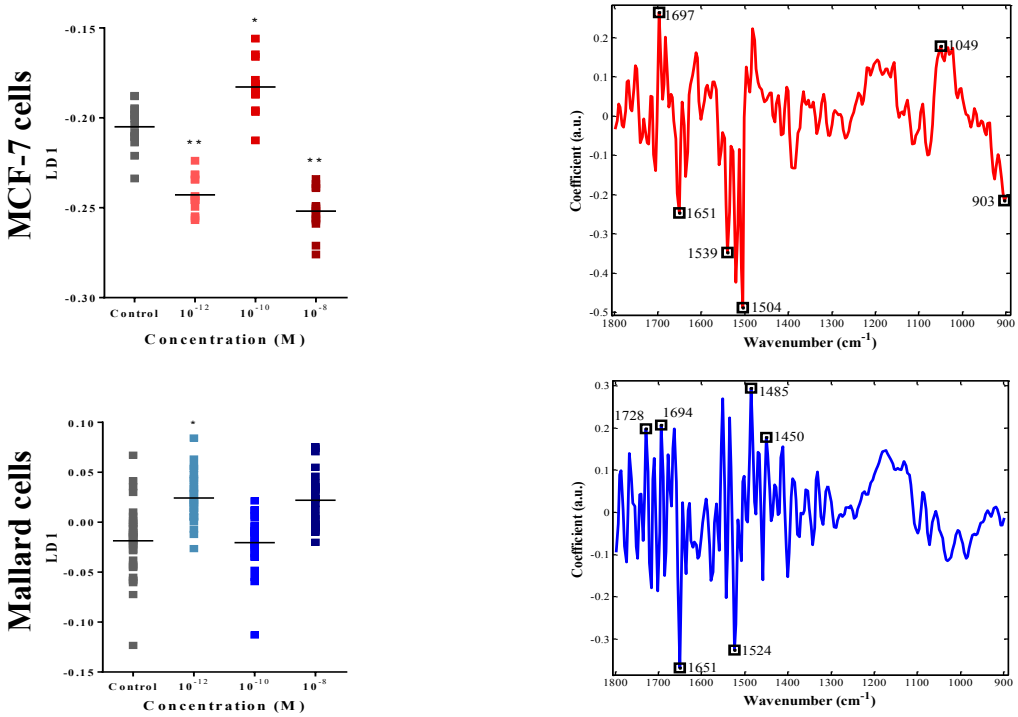

Figure 7